npj | Quantum Materials

www.nature.com/npjquantmats

ARTICLE OPEN

Unusual magnetic field-dependence of a possible hidden order phase

Eleonir João Calegari[1], Sergio Garcia Magalhaes[2] and Peter S. Riseborough[3]

URu_2Si_2 exhibits a second-order phase transition at 17.5 K. Initially it was thought that the transition was to a spin density wave phase, however, subsequent measurements do not support this assignment. Despite the unknown nature of the order parameter, many experimental results can be described in terms of the formation of a generic density wave. Here, we report calculations on an unusual phase of the underscreened Anderson lattice model, the so called spin-dependent inter-orbital density wave that has been proposed as describing the "hidden order" phase of URu_2Si_2. We determine the effects of an applied magnetic field. Since the order parameter describes an ordering in the x–y plane, the electronic properties of the system are anisotropic below the critical temperature T_{HO}. We show that the magnetic susceptibility becomes anisotropic below T_{HO}. Furthermore, for fields applied along a spontaneously chosen hard axis, T_{HO} decreases towards zero and that the HO transition changes from second order to first order at a large value of the magnetic field. Also, we find that the system undergoes a cascade of field-induced Lifshitz transitions and also show how these properties originate from the dependence of the quasi-particle bands on the orientation of the applied field. The good qualitative agreement with experimental findings provides strong support for the proposed description of the HO phase as a spin-dependent inter-orbital density wave phase.

npj Quantum Materials (2017)2:48 ; doi:10.1038/s41535-017-0055-2

INTRODUCTION

Despite the 30 years that have elapsed since its discovery, the nature of the phase found in URu_2Si_2 below the critical temperature $T_{HO} = 17.5$ K[1, 2] remains unknown. This enigmatic low-temperature phase has come to be known as the "hidden order" (HO) phase. The HO transition is marked by the formation of a gap, which extends over 60% of the Fermi-surface.[2, 3] Initially, the transition was thought to lead to a conventional spin density wave phase. However, inelastic neutron scattering measurements ruled out this possibility.[4] Nevertheless, the application of pressure causes a large moment antiferromagnetic phase to appear.[5, 6] To complete the puzzling scenario, the preponderance of evidence indicates that no structural transition occurs.[7–9]

Over the years that have elapsed since its discovery, many theories have been advanced to describe the HO phase. The proposals include quadrupolar,[10, 11] octapolar[12, 13] and higher-order multipolar ordering.[14–16] The predictions based on quadrupolar orderings are inconsistent with resonant X-ray diffraction experiments.[17, 18] Observation of high-order multipolar ordering via either neutron or X-ray diffraction experiments may prove to be very difficult since, presently, this requires high-precision measurement of the form factors at high momentum transfers. Other recent proposed description of the ordered phase include, unconventional or d spin-density waves,[19] Pomeranchuk instabilities,[20] modulated spin liquids,[21] hybridization waves,[22] spin-nematic ordering[23] and hastatic ordering.[24] Since an $l = 1$ Pomeranchuk instability is subject to severe limitations[25] and since the Fermi-surface measured by ARPES and de Haas—van Alphen measurements show evidence of a doubling of the unit cell,[26–28] the proposal that the HO transition in URu_2Si_2 is a Pomeranchuk instability[20] may require revision to include either $Q \neq 0$ or $l > 1$. If the ordering involves a hybridization wave state,[22] this should be accompanied by a charge density wave,[29] which could have been expected to be detected in one of the many high-resolution scattering experiments that have been performed.[7–9] Hastatic ordering[24, 30] is accompanied by the formation of a static, in-plane, magnetization of the conduction electrons. The hastatic picture of URu_2Si_2 and the phenomenological picture of Rau and Kee,[31] which also predicts a static transverse moment, are not supported by the results of neutron scattering experiments[32–34] that have placed an upper limit on the value of a transverse moment which is an order of magnitude smaller than the predicted hastatic value of 0.015 μ_B. Due to the absence of a definitive identification of the symmetries that are broken at the HO transition, the nature of the HO phase remains an outstanding issue in heavy-fermion physics.[35, 36]

Here, we report an unusual magnetic field dependence of the properties found for a novel phase of the underscreened Anderson lattice (UAL) model[37] that was recently proposed to describe the HO phase of URu_2Si_2. The choice of an itinerant model is motivated by the absence of evidence of well-defined crystal field levels in inelastic neutron scattering data[38] and high-resolution inelastic X-ray scattering experiments, which indicate that the widths of any crystal field excitations are simply too large to be considered as excitations of a localized system.[39] The itinerant description is supported by the determination[40–42] that uranium 5f electrons are delocalized and have an occupation of about 2.7 electrons per uranium and the participation of heavy itinerant 5f electrons in the Fermi-surface.[28] Although there is

[1]Departamento de Física, Universidade Federal de Santa Maria, 97105-900 Santa Maria, Rio Grande do Sul, Brazil; [2]Instituto de Fisica, Universidade Federal do Rio Grande do Sul, 91501-970 Porto Alegre, Rio Grande do Sul, Brazil and [3]Physics Department, Temple University, Philadelphia, PA 19122, USA
Correspondence: Peter S. Riseborough (prisebor@temple.edu)

Received: 8 April 2017 Revised: 23 July 2017 Accepted: 31 July 2017
Published online: 29 August 2017

experimental evidence of hybridization between the 5*f* electrons and the conduction electrons,[43, 44] electronic structure calculations indicate that the bands near the Fermi-energy are primarily of 5*f* character.[45] Nevertheless, small admixtures of conduction band character are found. Since there appears to be a scarcity of conduction electron weight in the vicinity of the Fermi-energy which is required for the hybridization to either completely screen[46] or delocalize the 5*f* moments,[47] the UAL model seems apt.[48] However, the UAL model needs to be modified by the inclusion of hopping processes whereby electrons are directly transferred between the 5*f* orbitals on neighboring atoms.[37] It is the delocalization of all the 5*f* states caused by the inter-site hopping process that counteracts the tendency for residual 5*f* local moments to order.

The new feature of our approach is that the candidate order parameter (OP) for the HO phase[37] reflects a very peculiar type of broken symmetry in the UAL model, i.e., a broken spin-rotational symmetry without the formation of a magnetic moment. The broken symmetry is driven by the spin-flip part of the Hund's rule interaction of the UAL model. The candidate OP is given by the expectation value of the non-hermitian operator $\hat{z}^{\chi'\chi}_{\underline{Q},\sigma}$ ($\underline{Q}$ is the fixed commensurate nesting vector) defined as

$$\hat{z}^{\chi'\chi}_{\underline{q},\sigma} = \frac{1}{N}\sum_{\underline{k}} f^{\dagger,\chi'}_{\underline{k}+\underline{q},\sigma} f^{\chi}_{\underline{k},\sigma}, \tag{1}$$

which leads to a low-temperature phase that can be described as a spin-dependent inter-orbital density wave. More specifically, the ordering produces a state characterized by an inhomogeneous, spin-dependent mixing of *f* states with different orbital characters given by χ. It should be remarked the non-trivial spin dependence of the OP,[37]

$$z^{\chi'\chi}_{\underline{Q},\sigma} = -z^{\chi'\chi}_{\underline{Q},-\sigma}. \tag{2}$$

The OP is the expectation value of a non-Hermitean operator and, therefore, does not correspond to a measurable quantity. The proposed HO state does globally break a gauge-invariance of the Hamiltonian. The transition spontaneously generates a phase difference between the different 5*f* components of the wave function and, as such, can be considered as breaking chiral (axial) gauge invariance. Due to the relation displayed in Eq. (2) and the quenching of the orbital angular momentum, the phase with a purely imaginary OP, $z^{\chi',\chi}_{\underline{Q},\sigma} = \exp\left[\pm i\frac{\pi}{2}\right] r$ results in the HO state being time-reversal invariant. This is easily seen since the Wigner time-reversal operator $\mathcal{T}$ defined by

$$\mathcal{T} = \exp\left[-i\frac{\pi}{2}\sigma_y\right]\kappa, \tag{3}$$

where κ denotes complex conjugation, transforms the up-spin states into the down-spin states. However, general complex values of $z^{\chi',\chi}_{\underline{Q},\sigma}$ produce identical magnetic properties since the orbital angular momentum is quenched by the hopping. In this respect, the itinerant UAL model is different from the model considered by Haule and Kotliar.[14] The two time-reversal invariant chiral states have properties similar to those found in Raman scattering experiments[49] since the two degenerate states both preserve time-reversal invariance, have no net spin, and have the same charge character. However, unlike the chiral states of Kung et al.,[49] the relation between UAL chiral states to reflection symmetry is, as yet, undetermined. The time-inversion invariance of the HO order phase is not only supported by the results of Kung et al.[49] but also by recent Polar Kerr effect (PKE) measurements.[50] The PKE experiments identified a large field-trainable effect in the superconducting state but only showed a small signal at the HO transition which was attributed to the existence of parasitic phases.[51–53]

The present work is aimed at the investigation of the consequences that the application of a magnetic field have on the ordered phase. The results of this work support the suggestion that the OP $z^{\chi,\chi'}_{Q}$, which appears as a result of the spontaneous breaking of spin-rotational invariance, is at work in URu_2Si_2. All our results can be traced directly to the behaviour of the 5*f* quasi-particle dispersion relations. The unusual nature of these dispersion relations follows from the peculiar spin-rotational symmetry breaking that is driven by the *x* and *y* components of the Hund's rule interaction in the UAL model. Since the ordering involves the *x* and *y* components of the Hund's rule interaction, the ordering produces a hard-axis and an easy-plane but does not produce an ordered magnetic moment. As a consequence, the quasi-particle dispersion relations of the HO phase are found to be affected differently by magnetic fields applied in the easy magnetic direction (*x*-axis) as opposed to the hard magnetic direction (*z*-axis).

The temperature versus magnetic field phase diagram and the anisotropy found in magnetic torque measurements are believed to be crucial ingredients for the discover of the identity of the HO phase. Therefore, they are important constraints for any candidate theory for the elucidation of the HO phase in URu_2Si_2. In the first case, the experimental field dependence of T_{HO} displays different behaviour for fields applied along the tetragonal *c* and *a* axes. For the *c*-axis, T_{HO} decreases when the field is increased. However, for the *b*-axis T_{HO} is only weakly affected.[54] Moreover, the application of large magnetic fields along the tetragonal *c*-axis of URu_2Si_2 shows that the HO phase is destroyed at around 35 T. The second-order boundary line between the non-magnetic HO and the normal-paramagnetic phase is replaced by a first-order one around 25 T.[55, 56] For fields between 35 and 40 T, the *T*–*H* phase diagram contains a dome of an unknown phase. In the case of magnetic torque measurements,[57] it has been reported that, below the ordering temperature, the linear susceptibility becomes anisotropic in the tetragonal *a*–*b* plane suggesting that the four-fold rotational symmetry is broken in the low-temperature phase. Since the underlying crystal apparently remains tetragonal,[9] the nematic phase is expected to have a purely electronic origin. Moreover, the experimental findings[58] for the non-linear susceptibility χ_3 as function of temperature shows a sharp anomaly at $T = T_{HO}$ for the fields parallel to the tetragonal *c*-axis whereas it has a very weak temperature dependence for fields perpendicular to the *c*-axis.

It is to be noted that since this work uses cubic symmetry, the results only depend on the direction of the magnetic field relative to the hard magnetic direction and not to the crystallographic axes (denoted by *a*, *b* and *c*). This hinders direct comparision with experimental results on URu_2Si_2. Nevertheless, the particular form of rotational symmetry breaking in our theory produces a spontaneous selection of an easy-plane and hard axis which can lead to anisotropic responses for applied magnetic field resembling those found in the URu_2Si_2.

The paper is structured as follows: in section II we introduce the model and calculate the free energy, and present a detailed discussion of the results. The conclusions are presented in the last section.

RESULTS

We use the UAL model which describes two degenerate localized 5*f* bands (labeled by $\chi = \alpha, \beta$), which acquire itinerant character by direct hopping between neighboring 5*f* shells and by their mixing with one itinerant conduction band with dispersion relation $\epsilon_d(\underline{k})$. The two degenerate narrow *f* bands exhibit intraband and interband nesting $E^{\alpha}_{f}(\underline{k}+\underline{Q}) = -E^{\alpha(\beta)}_{f}(\underline{k})$. The *f* electrons interact

via local Coulomb and exchange interactions

$$\begin{aligned}\hat{H}_f &= \left(\tfrac{U-J}{2N}\right)\sum_{\underline{k},\underline{k}',\underline{q}}\sum_{\sigma}\sum_{X\neq X'} f^{\dagger,X}_{\underline{k}+\underline{q},\sigma} f^{X}_{\underline{k},\sigma} f^{\dagger,X'}_{\underline{k}'-\underline{q},\sigma} f^{X'}_{\underline{k}',\sigma} \\ &+\left(\tfrac{U}{2N}\right)\sum_{\underline{k},\underline{k}',\underline{q}}\sum_{\sigma}\sum_{X,X'} f^{\dagger,X}_{\underline{k}+\underline{q},\sigma} f^{X}_{\underline{k},\sigma} f^{\dagger,X'}_{\underline{k}'-\underline{q},-\sigma} f^{X'}_{\underline{k}',-\sigma} \\ &+\left(\tfrac{J}{2N}\right)\sum_{\underline{k},\underline{k}',\underline{q}}\sum_{\sigma}\sum_{X\neq X'} f^{\dagger,X}_{\underline{k}+\underline{q},\sigma} f^{X'}_{\underline{k},\sigma} f^{\dagger,X'}_{\underline{k}'-\underline{q},-\sigma} f^{X}_{\underline{k}',-\sigma}\end{aligned} \quad , \tag{4}$$

where N is the number of sites. At the mean-field level, where the fluctuations in $\hat{z}^{XX'}_{\underline{q},\sigma}$ and $\hat{n}^{X}_{f,\sigma}$ (the f-electron occupation number operator) are considered as small, the free energy is given as:

$$\begin{aligned}F &= -k_B T\sum_{\underline{k},\sigma}\sum_{j}\left[\ln\left(1+e^{-\beta\left(E^{(j)}_{\sigma}(\underline{k})-\mu\right)}\right)\right]+\mu N_{\text{elec}} \\ &-N\sum_{\sigma}\sum_{X\neq X'} z^{XX'}_{\underline{Q},\sigma}\kappa^{X'X}_{\underline{Q},\sigma}\end{aligned} \tag{5}$$

and $\kappa^{X'X}_{\underline{Q},\sigma}$ is a complex number defined by

$$\kappa^{X'X}_{\underline{Q},\sigma} = Jz^{X'X}_{-\underline{Q},-\sigma} - (U-J)z^{X'X}_{\underline{Q},\sigma}, \tag{6}$$

where the non-zero $z^{X'X}_{-\underline{Q},\sigma}$ gives the novel spin-dependent inter-orbital density wave reflecting the breaking of the spin rotationally invariance within the Hund's rule part of the interaction.

The quasi-particle dispersion relations $E^{(j)}_{\underline{k},\sigma}$ for electrons of spin σ satisfy

$$\det[\omega\underline{I} - \underline{\Lambda}_{\sigma}(\omega,\underline{k})] = \prod_{j}\left[\omega - E^{(j)}_{\sigma}(\underline{k})\right] = 0, \tag{7}$$

where $\underline{I}$ is the identity matrix and the matrix $\underline{\Lambda}_{\sigma}(\omega,\underline{k})$ is given below

$$\begin{pmatrix} -E^{\beta}_{f,\sigma}(\underline{k}) & \left(\kappa^{\beta\alpha}_{\underline{Q},\sigma}\right)^{*} & -h_x & 0 & 0 & V_a \\ \kappa^{\beta\alpha}_{\underline{Q},\sigma} & E^{\beta}_{f,\sigma}(\underline{k}) & 0 & -h_x & 0 & 0 \\ -h_x & 0 & -E^{\beta}_{f,\sigma}(\underline{k}) & -\left(\kappa^{\beta\alpha}_{\underline{Q},\sigma}\right)^{*} & V_a & 0 \\ 0 & -h_x & -\kappa^{\beta\alpha}_{\underline{Q},\sigma} & E^{\beta}_{f,\sigma}(\underline{k}) & 0 & 0 \\ 0 & 0 & V^{*}_a & 0 & \epsilon_{\sigma}(\underline{k}) & -h_x \\ V^{*}_a & 0 & 0 & 0 & -h_x & \epsilon_{\sigma}(\underline{k}) \end{pmatrix},$$

where $h_{x(z)} = \sigma\mu_B H_{x(z)}$ and $E^{X}_{f,\sigma}(\underline{k})$ is given by

$$E^{X}_{f,\sigma}(\underline{k}) = E^{X}_{f}(\underline{k}) - h_z + \sum_{X'}\left[(U-J)n^{X'}_{f,\sigma}\left(1-\delta^{XX'}\right)+Un^{X'}_{f,-\sigma}\right] \tag{8}$$

$\epsilon_{\sigma}(\underline{k}) = \epsilon_{d}(\underline{k}) - h_z$ and $E^{X}_{f}(\underline{k}) = E_f + \epsilon_f(\underline{k})$, where

$$\epsilon_s(\underline{k}) = -2t_s\left[\cos(k_x a)+\cos(k_y a)+\cos(k_z a)\right] \tag{9}$$

in which s =f or d, and a is the lattice parameter. The gyromagnetic factors are assumed to be equal, i.e., $g_f = g_d = 1$. The OP $z^{\alpha\beta}_{\underline{Q},\sigma}$ can be obtained from the free energy on minimizing F with respect to $z^{\beta\alpha}_{-\underline{Q},-\sigma}$. We define the susceptibility g_σ for the OP via $z^{\alpha\beta}_{\underline{Q},\sigma} = -g_\sigma\kappa^{\beta\alpha}_{\underline{Q},\sigma}$. The tight-binding parameter values used in the calculations in the next section correspond to $t_d = -1/6$, $t_f = 1/20$ and $V = 1/10$ eV. These values were chosen as generic values but give rise to a width $2W_f$ of the $5f$ band due to direct $5f$ hopping of 0.6 eV which is a little smaller than the $5f$ band widths of ≈1 and 1.5 eV determined, respectively, by DFT + DMFT[14] and DFT[45] calculations. Apart from raising the degeneracy of the α and β bands, the value of V has little effect on the results. The value of the effective f level energy E_f was chosen to be 0.3 eV and the value of $\mu(T,H)$ was determined to be around 0.32, so that the $5f$ bands will be approximately half-filled. The values of U and J were chosen to be equal, in order to avoid an unnecessary increase the number of parameters of the theory. However, estimates of the ratio J/U found in the literature range from 0.49[45] to 0.14.[14] We find that smaller values of the ratio have the effect of increasing the stability of the HO phase wrt a neighbouring AF phase that is stable at smaller W_f values. The value of $U = 0.074$ eV was chosen in order to give $T_{HO} = 17.5$ K and corresponds to a ratio $U/W_f \approx 0.25$ which is close to the range 0.26–0.4 used in ($J = 0$) DFT + DMFT calculations.[45] Throughout the calculations, a commensurate value of $\underline{Q}$ was used. This fixed value was used since it was observed that at $H = 0$, (i) the HO instability criterion is dominated by electron–hole processes with energies greater than k_BT and, hence, is insensitive to the precise form of the dispersion relations at the Fermi-energy, (ii) commensurate ordering produces greater condensation energies than the neighboring incommensurate phases due to the effect of multiple scattering processes and (iii) at finite fields, the HO instability involves equal spin electron–hole pairs and, thus, $\mu_B H$ is expected to act as a low-energy cut-off in the gap equation much in the same way as k_BT does.

Figure 1 shows the specific heat C_v obtained from the free energy given in Eq. (5). The specific heat is shown for different magnitudes of the magnetic field H_z. The jump in the specific heat marks the temperature at which the transition to the HO phase occurs. For finite applied magnetic fields $H_z > 0.0$ T, the jump in C_v is shifted to lower temperatures and for $H_z \gtrsim 28.0$ T the anomaly becomes sharper indicating that the system is approaching a regime of first-order transitions.

The first-order nature of the transition inferred from the specific heat shown in Fig. 1 is confirmed by the analysis of the free energy as function of the HO OP $z^{X'X}_{\underline{Q},\sigma}$. For the particular case in which $U = J$, a non-trivial solution for $z^{X'X}_{\underline{Q},\sigma}$ must satisfy the condition $J^2F_\sigma = 1$ in which $F_\sigma = g_\sigma g_{-\sigma}$. Figure 2a shows the quantity J^2F_σ versus $z^{X'X}_{\underline{Q},\sigma}$ for different values of H_z. For $H_z = 20.0$ T; there is only one non-trivial solution ($z_{Q,\sigma} \neq 0$) s_1 indicating that the system is in a regime of second-order transitions. However, for $H_z = 33.0$ T there are two non-trivial solutions, s_1 and s_2, characterizing a regime of first-order transitions. Figure 2b shows the behavior of the free energy per unit cell ($f = F/N$) for $H_z = 32.0$ T and for the temperature $T = 2.0$ K ($< T_{HO} = 3.48$ K). The solution s_2 always corresponds to a maximum of the free energy, therefore, it

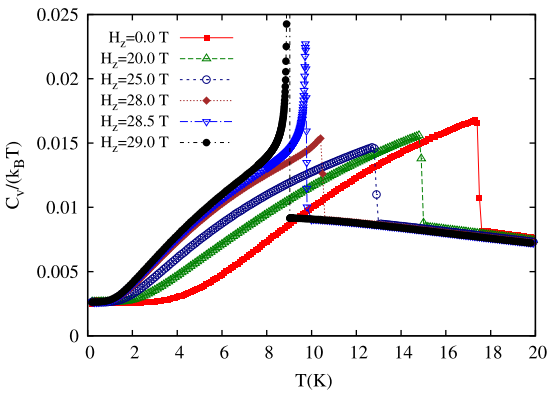

Fig. 1 Behavior of the C_v for several values of the magnetic field H_z. For $H_z = 0.0$ T, the jump in the specific heat has the value of $\Delta C_v = 1.285 \times 10^{-5}$ eV/K/atom

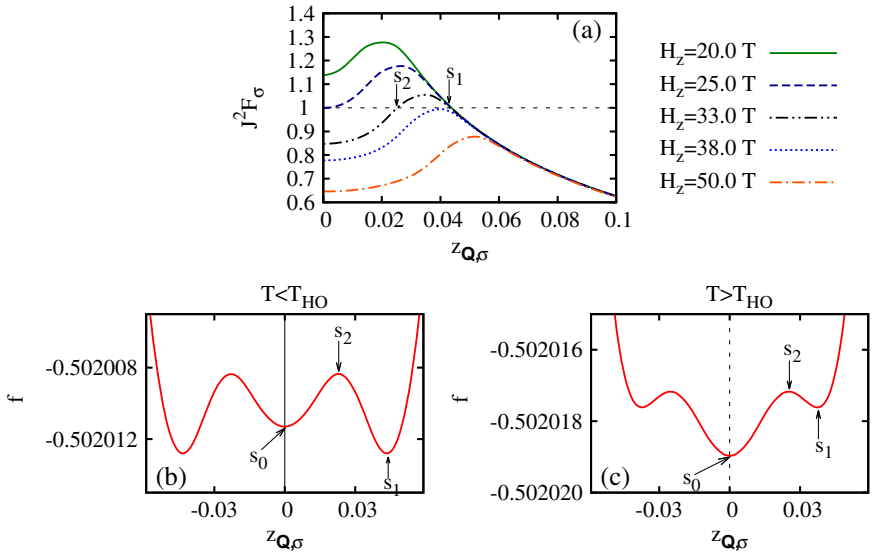

Fig. 2 In **a**, the J^2F_σ (see the text) versus the order parameter $z_{Q,\sigma}$ for $T = 2.0$ K and different magnitudes of H_z. The s_1 and s_2 indicate the non-trivial solutions, while s_0 shows the trivial solution in the region of first-order transition. In **b** the free energy per unit cell ($f = F/N$) versus $z^{\chi\chi}_{Q,\sigma}$ for $T = 2.0$ K and $H_z = 32.0$ T. **c** shows the free energy f for $T = 5.0$ K and $H_z = 32.0$ T

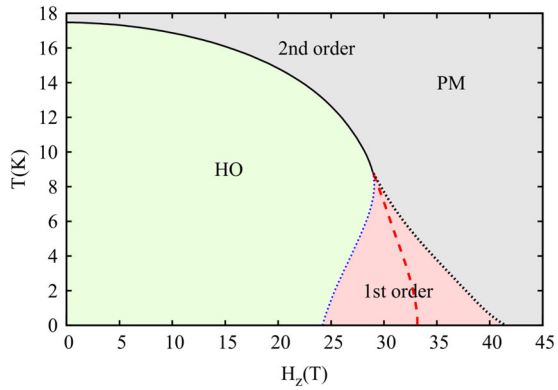

Fig. 3 Phase diagram T_{HO} versus magnetic field H_z for $U = J = 0.074$ eV and $V = 1/10$ eV

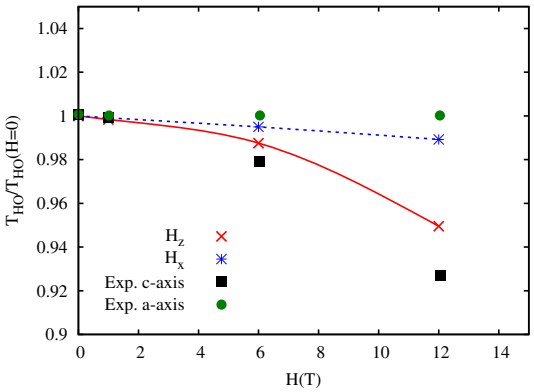

Fig. 4 The field dependence of the temperature T_{HO} normalized by the zero field transition temperature $T_{HO}(H = 0)$. The squares show the experimental result[54] for fields along the *c*-axis while the circles show the experimental result[54] for fields along the *a*-axis

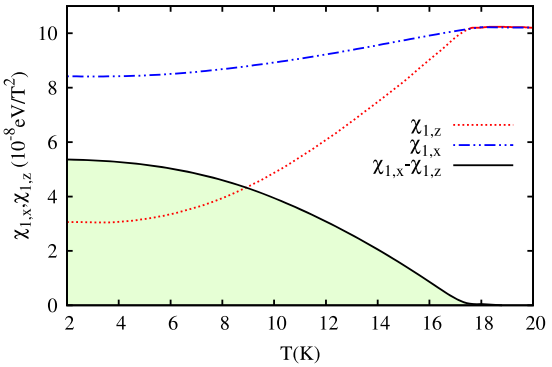

Fig. 5 The linear susceptibility $\chi_{1,z}$, $\chi_{1,x}$ and $\chi_{1,x} - \chi_{1,z}$ versus temperature

is sufficient to only compare the stability of the trivial solution s_0 and the non-trivial solution s_1. Figure 2c shows the free energy f for $H_z = 32.0$ T and $T = 5.0$ K. Since $T > T_{HO}$, the solution s_0 is the more stable one.

From the minima of the free energy, one can construct the T–H_z phase diagram. The phase diagram is displayed in Fig. 3. The solid line marks second-order transitions between the HO (HO) and the paramagnetic (PM) phases. The dashed line at low temperature and high magnetic field marks first-order transitions. The dotted lines are the spinodal lines which mark the boundaries of the regions where multiple solutions for the OP $z_{Q,\sigma}$ are found (see Fig. 2a). The values of H_z and T which describe the first-order and spinodal lines were determined from the free energy, which has forms similar to those shown in Fig. 2. The field scale that determines the switch from second-order to first-order is determined by twice the energy difference between the energy at which the commensurate nesting would be optimal and the actual value of the Fermi-energy. At this field, the condensation energy due to the commensurate scattering no longer sufficiently balances the entropy change. Since the mean-field approximation is not expected to be valid within the Ginzberg critical regime, the effects of commensurate and incommensurate fluctuations should be investigated further.

Figure 4 displays the dependence of T_{HO} on the orientation of the magnetic field, i.e., H_z and H_x. The results are compared with the experimental finding of Pfleiderer et al.[54] For fields along the

z-axis, T_{HO} decreases when H_z increases. By contrast, T_{HO} is only weakly affected when H_x is applied.

The linear susceptibility is obtained as the second-derivative of the free energy. Figure 5 shows χ_1 for both the H_x and H_z magnetic fields. The derivatives were performed numerically. Our results shows that, at low temperatures, $\chi_{1,z}$ has a weaker temperature dependence than $\chi_{1,x}$. However, as $T \to T_{HO}$, $\chi_{1,z}$ increases rapidly in such way that, at $T = T_{HO}$, $\chi_{1,z} = \chi_{1,x}$. This temperature behaviour is in agreement with experimental results[57] for URu_2Si_2. The green region in Fig. 5 shows the difference $\chi_{1,x} - \chi_{1,z}$ stressing the

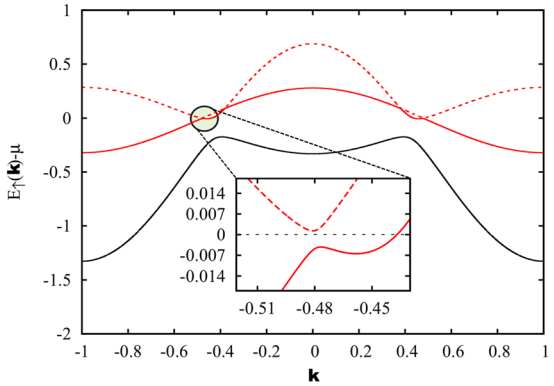

Fig. 6 The spin-up quasi-particle bands for α electrons at $T = 0$ and $H_z = 20$ T for the direction $\bar{A} - \Gamma - A$ with $\bar{A} = (-\pi, -\pi, -\pi)$, $\Gamma = (0, 0, 0)$ and $A = (\pi, \pi, \pi)$. The inset shows in detail the gap between the folded β-band and the hybridized α-band

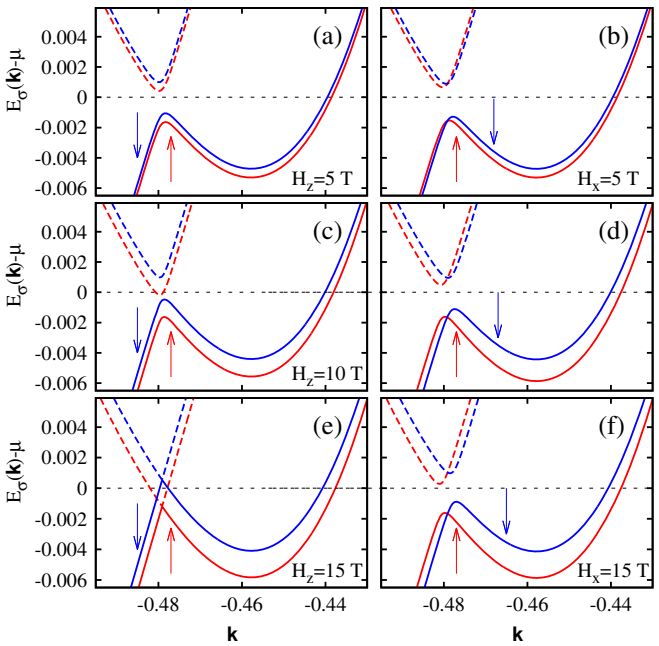

Fig. 7 The polarized quasi-particle dispersion relations for the α electrons at $T = 16.5$ K, $U = J = 0.074$ eV, $V = 1/10$ eV, $\mu = 0.32$ eV and different fields that are applied either in the z-direction or x-direction. The up arrows indicate the spin-up bands represented by the red lines while the down arrows indicate the spin-down bands denoted by the blue lines. The dashed lines indicate the position of the chemical potential

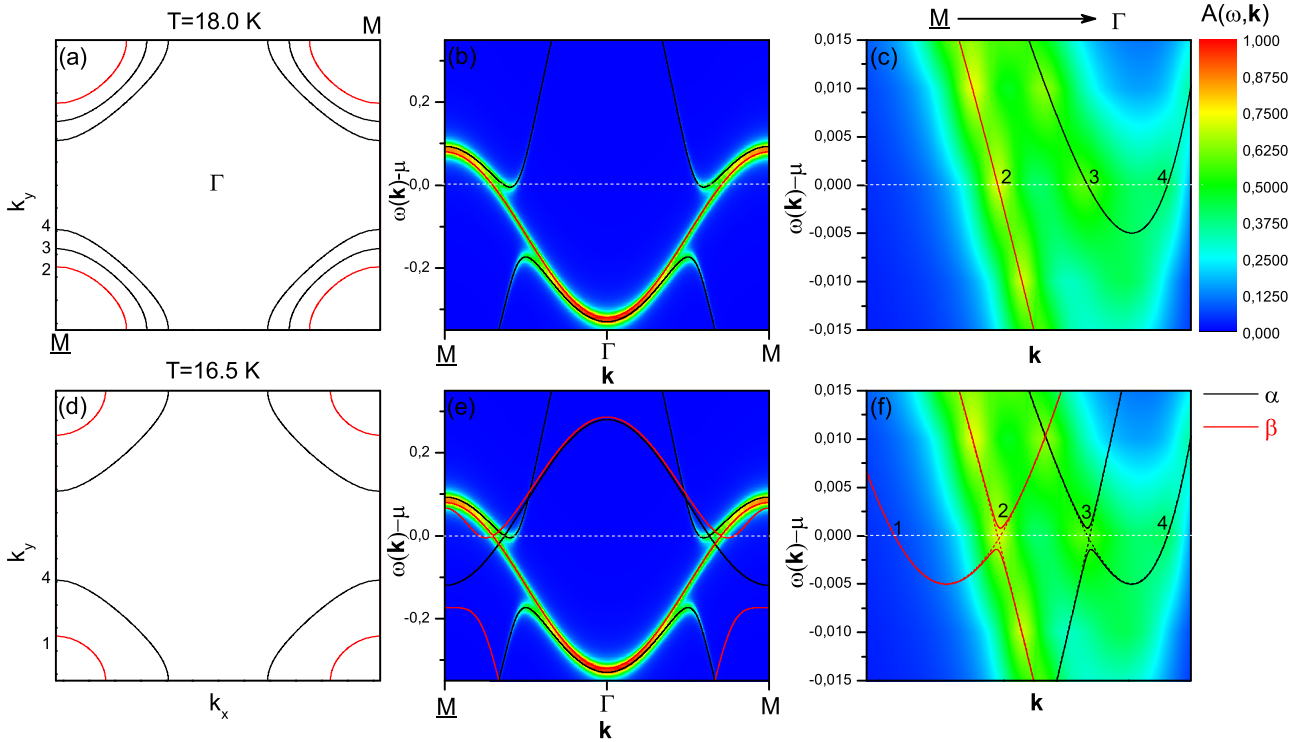

Fig. 8 In **a**, **d**, a cross-section of the Fermi surfaces in the $k_z = 0$ plane for two different temperatures and magnetic field ($H_z = 0$ T). In **b**, **e** the lines show the quasi-particle bands $E_\sigma^{(j)}(\underline{k})$ along the high symmetry direction $\underline{M}$-Γ-M with $\underline{M} = (-\pi, -\pi, 0)$, $\Gamma = (0, 0, 0)$ and $M = (\pi, \pi, 0)$. The colors exhibit the spectral function $A(\omega, k)$. The panels **c**, **f** show in details the gapped region of the quasi-particle bands along the direction $\underline{M}$-Γ

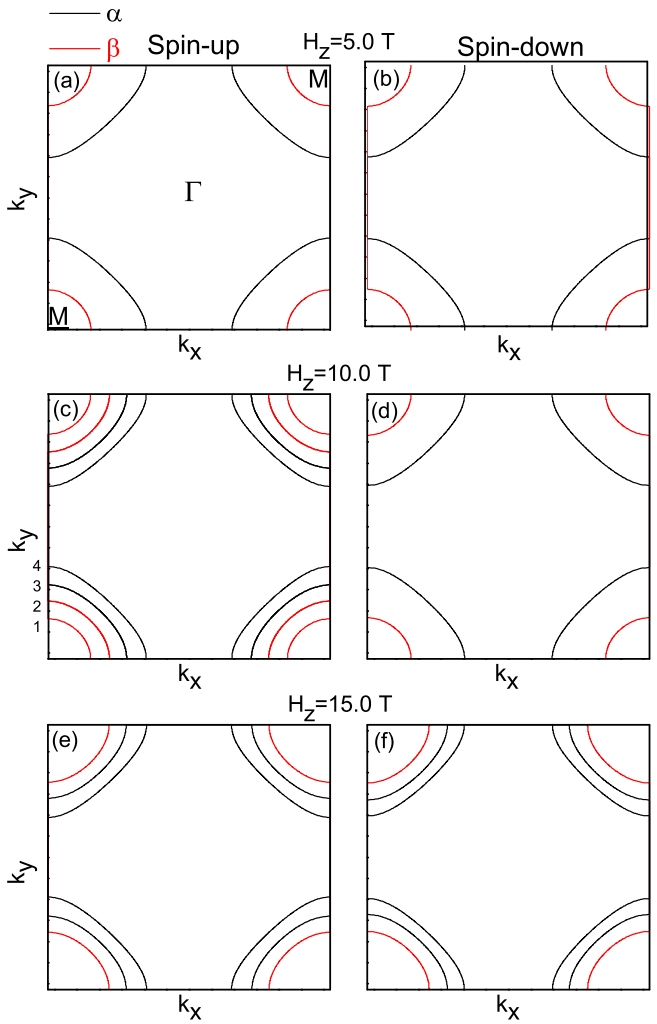

Fig. 9 In **a**, **c**, **e**, a cross-section of the spin-up Fermi surfaces in the $k_z = 0$ plane for the same magnetic fields (H_z) as in Fig. 7. In **b**, **d**, **f**, the spin-down Fermi surfaces. The temperature and the model parameters are the same as in Fig. 7

dependence of the linear susceptibility on the field orientation and temperature.

DISCUSSION

The results for T_{HO} and χ_1 discussed above can also be explained by the analysis of the quasi-particle dispersion relations. Figure 6 shows the spin-up quasi-particle bands $E_{\uparrow}^{(j)}(\underline{k})$ for the α electrons at $T = 0.0$ K and $H_z = 20$ T over the entire diagonal of the Brillouin zone $(-\pi, -\pi, -\pi) - (\pi, \pi, \pi)$. The circle highlights the gapped region that is shown in the inset. Figure 7 shows the polarized quasi-particle bands $E_{\sigma}^{(j)}(\underline{k})$ for the α electrons, in the vicinity of the HO gap for temperatures close to T_{HO}. The up arrows indicate the spin-up sub-bands represented by the red lines while the down arrows indicate the spin-down sub-bands denoted by the blue lines. The Fig. 7a, c, e shows the effect of fields oriented along the z-direction on the HO gap for $T = 16.5$ K. Inspection of the quasi-particle bands reveals that the behavior of T_{HO} observed in Fig. 4 comes from the combined effects of the magnetic field and temperature. By increasing the field H_z, the Zeeman splitting between the spin-up and spin-down sub-bands increases, while the closing of the gap is mainly caused by increasing temperature and, to a lesser extent, the raising of the magnetic field. We note that as the field is increased beyond $H_z = 10$ T the up spin band falls below the Fermi-energy, indicating a change in Fermi-surface topology known as a Lifshitz transition. For $H_z = 15$ T the gap between the spin-up and spin-down band has closed and the HO state has been destabilized. The initial slow field-dependence of the gap reflects the fact that, close to the (gapped) nesting point, the contributions of the Zeeman energy to the free energy cancel exactly. This cancellation occurs as long as the upper spin-up band and the lower spin-down band do not cross the Fermi-energy and produce electron and hole pockets. Hence, the dominant initial H_z^2-dependence of the gap originates from the states with other $\underline{k}$ values at which the reconstructed bands cross the Fermi-energy. However, since these other states are only weakly coupled to the states at the nesting points $\underline{k} = \pm \underline{Q}/2$, the initial field-dependence of the gap is small but accelerates when electron and hole pockets are formed. Likewise, since the resulting H_z^2 term in the free energy originating from the quasi-particle bands only comes from a restricted range of $\underline{k}$, the linear susceptibility $\chi_{1,z}$ is correspondingly small. The Fig. 7b, d, f shows the change in the quasi-particle bands caused by a field oriented along the x-direction when $T = 16.5$ K. By contrast to the H_z case, the main effect of the H_x field is to not to produce a Zeeman splitting but instead produces a spin-dependent momentum-shift of the quasi-particle bands. The spin-dependent momentum shifts are produced by H_x which couples the spin-up and spin-down states that are comprised of spin-dependent admixtures of states with $\underline{k}$ and $\underline{k} \pm \underline{Q}$. Therefore, to second-order in H_x, the field produces a lowering of the quasi-particle energies that is most prominent where the admixture associated with the HO OP is large. Thus, as seen in Fig. 7, the magnitudes of the gaps $\Delta_{\uparrow}$ and $\Delta_{\downarrow}$ and T_{HO} are only slightly dependent on H_x. As a result, the bottom of the up-spin band reaches the Fermi-energy at practically the same temperature as at $H_x = 0.0$ T. Therefore, the formation of electron and hole pockets are dominantly caused by temperature variation and hardly depend of H_x. The above observations explain the distinct behaviors of T_{HO} seen in Fig. 4. Likewise, since the energy lowering from the H_x field is proportional to H_x^2 and since it comes from the both the gapped and non-gapped regions of $\underline{k}$ space, the linear susceptibility $\chi_{1,x}$ is greater than $\chi_{1,z}$.

The Fermi surfaces for $H_z = H_x = 0$ T are shown for two different temperatures (above and below $T_{HO} = 17.5$ K) in Fig. 8. In 8a, $T = 18.0$ K, the black lines show the Fermi surface for the α electrons, while the red line shows the Fermi surface for the β electrons. In Fig. 8b, the quasi-particle bands for the α (black) and β (red) electrons are shown for the same temperature as in Fig. 8a. The color map shows the spectral function $A(\omega,k)$ for each one of the quasi-particle bands. Figure 8c shows in detail the region where the quasi-particle bands intercept the chemical potential at the points 2, 3 and 4 along the direction $\underline{M}$-Γ. Point 2 is associated to the Fermi surface of the β electrons while points 3 and 4 correspond to the Fermi surfaces of the α electrons (see Fig. 8a). Figure 8d show the Fermi surfaces for HO state with $T = 16.5$ K, while Fig. 8e exhibits the quasi-particle bands and the spectral function for the same temperature as in Fig. 8d. The comparison of the Fig. 8a, d show that when the system enters in the HO state the Fermi surface is reduced significantly. Above T_{HO} (see Fig. 8a) there are three branches of Fermi surface, two from the hybridized $\alpha - f$ and d band and one from the unhybridized $\beta - f$ band. Below T_{HO} (see Fig. 8d), the hybridized band $\alpha - f$ with wave vector $\underline{k}$ mixes with the unhybridized band $\beta - f$ at $\underline{k} + \underline{Q}$ as shown in Fig. 8e. Two bands become gapped as in Fig. 8f and, therefore, there are only two branches of Fermi surface in the HO state. Moreover, the spectral weight of one of the branches (the *red one*) is very small as shown at the point 1 of Fig. 8f. Therefore, it can be concluded that about 60% of the Fermi-surface has been lost when the system enters in the HO state.

The reconstruction of the Fermi surface in applied field is shown in the field-induced changes of the Fermi-surface topology are

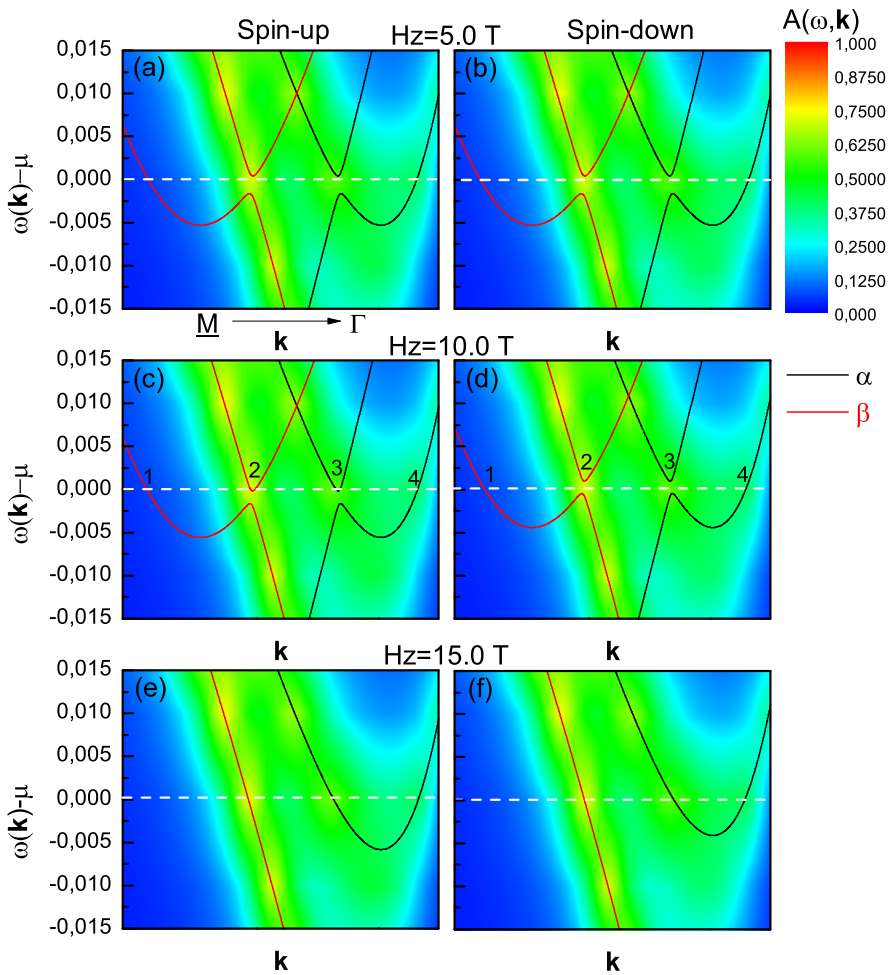

Fig. 10 The panels **a**, **c**, **e** show in details the gapped region of the spin-up quasi-particle bands along the direction $\underline{M} = (-\pi, -\pi, 0) - \Gamma = (0, 0, 0)$ while **b**, **d** and **f** show the spin-down quasi-particle bands. The model parameters and the temperature are the same as in Figs. 7 and 9

seen in Fig. 9. This process can be better understood through the analysis of the quasi-particle bands. Figure 10 show the quasi-particle bands for a small range of the wave vector k along the direction $\underline{M}$-Γ. In Fig. 10a, b, the situation is the same as in the case of $H_z = 0$ and temperature below T_{HO}, i.e., two bands become gaped, therefore there are only two branches of Fermi surface (see Fig. 9a, b). Figure 10c show the spin-up quasi-particle bands for $H_z = 10.0$ T. Notice that the magnetic field H_z shifted the bands to lower energies and as a consequence the bands are intercepted by the chemical potential also at points 2 and 3, in addition to points 1 and 4. Therefore, there are four branches for the spin-up Fermi surface as shown in Fig. 9c, but, taking into account that the branch associated to the point 1 has very small spectral weight, it can be considered that only three branches remain as in the normal state. On the other hand, in Fig. 10d the bands are shifted up by the magnetic field, but not sufficiently to intercept the chemical potential at the points 2 and 3. Thus the spin-down Fermi surface for $H_z = 10.0$ T has only two branches as shown in Fig. 9d. The comparison of Fig. 9c, d shows that under an applied magnetic field, due to the band polarization, the reconstruction of the Fermi surface is asymmetric, that is, the spin-up Fermi surface reconstructs before the spin-down Fermi surface. For $H_z = 15.0$ T the magnetic field suppresses the HO state and the structure of the quasi-particle bands of the normal state is recomposed as shown in Fig. 10e, f, and therefore the Fermi surface is completely reconstructed (see Fig. 9e, f). However, due to the polarization of the bands by the magnetic field, the spin-up Fermi surface is more populated than the spin-down one, consequently, the spin-up Fermi surface has a volume greater than the spin-down Fermi surface. To summarize, we have found the application of a magnetic field to the HO state may result in a cascade of changes in the topology of the Fermi surface. The sequence of field-induced Lifshitz transitions has been reported in the literature.[59, 60]

In addition to describing the above effects, the theory predicts that the density of states (DOS) measured in scanning tunneling microscope (STM) tunneling experiments in field should show marked differences when the field is applied either parallel or perpendicular to the director. The change in the DOS is intimately related to the dependence of the quasi-particle bands on the orientation of the field. Our zero-field calculated DOS shows asymmetric peaks around the partial gap caused by the HO, in accordance with measurements.[61] For fields along the hard-axis, our results show that the asymmetric peaks will spin-split, thereby lowering the Kramer's degeneracy. On the other hand, fields in the easy-plane should not produce spin-splitting and the gap structure should closely resembles the H = 0 structure. This type of STM experiment requires a highly-symmetrical tip and the capability of rotating either the field in the a-b plane or the sample's surface and, therefore, is quite demanding.

To complete our discussion, in Fig. 11a, b are displayed, respectively, the non-linear susceptibility χ_3 and the ratio χ_3/χ_1 for

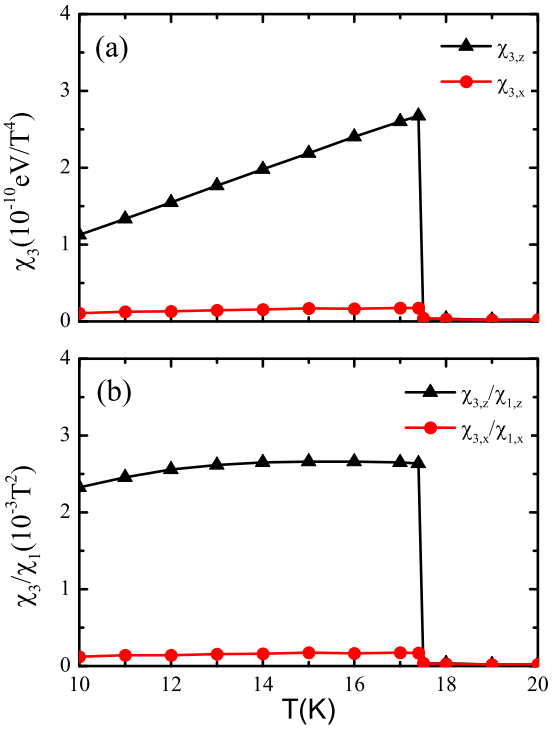

Fig. 11 **a** χ_{3z} and χ_{3x} as function of the temperature. **b** $(\chi_{3,z})/(\chi_{1,z})$ as a function of the temperature

both z and x axes. Our results show that the $\chi_{3,z}$ and $\chi_{3,x}$ have, respectively, a large sharp discontinuity and a very small step at $T = T_{HO}$. This behavior can be traced directly from χ_1 (see Fig. 5). From a broad view, such anisotropies are ultimately related to the way that the orientation of the magnetic field affects the OP introduced in Eq. (1). That can be seen quite clearly in the behaviour of T_{HO} shown in Fig. 4. From that result, one can conclude that there is a sharp discontinuity in χ_3 wherever T_{HO} is dependent on the field. On the other hand, such discontinuity tends to disappear in the direction of the field wherever T_{HO} has weak dependence on the field.

We have performed calculations on the UAL model that may describe the HO phase of URu_2Si_2. The magnetic properties, such as the susceptibility, become anisotropic below T_{HO}. We have shown that, for fields applied along a spontaneously chosen hard axis, T_{HO} decreases towards zero and that the HO transition changes from second order to first order at a large value of the magnetic field. This result is consistent with experimentally determined specific heat of URu_2Si_2.[55, 56] These features are consequences that the transition, driven by the spin-flip part of the Hund's rule interaction, spontaneously breaks the spin-rotational invariance. Furthermore, since the ordering involves the x and y components of the Hund's rule exchange, the ordering produces a preferential direction. Therefore, below T_{HO}, the quasi-particle bands depend on the orientation of the magnetic field. This feature produces the anisotropy in the system's properties, such as the magnetic susceptibility, which qualitatively agrees with experimental results[57] and gives support to the OP proposed[37] to describe the HO phase of URu_2Si_2. Results for the Fermi surface show that, under an applied field H_z, the reconstruction of the Fermi surface is anisotropic due to the band polarization. Finally, the non-linear susceptibility χ_3 exhibits a discontinuity at $T = T_{HO}$, similar to that observed in the specific-heat. The discontinuity is strongly dependent on the orientation of the magnetic field.

To conclude, the missing ingredient in our theory is the Ising anisotropy, which is not a unique feature of the HO phase since it already appears in the PM phase and large moment AFM phases.[62] Our simplified model cannot describe the anisotropy, without the addition of spin-orbit coupling and other ingredients such as the introduction of the set of Slater-Koster parameters t_σ, t_π, t_δ and t_ϕ that describe the anisotropic hopping of the 5f electrons. Nevertheless, even while not providing a detailed description of all the properties of URu_2Si_2, our results suggest that a variety of experimental results on this compound can be qualitatively understood in terms of one mechanism. Specifically, the spontaneous breaking of spin-rotational invariance driven by the Hund's rule interaction can qualitatively account for the unusual features found in experiments.

METHODS

All the numerical results were computed within a mean-field treatment of Coulomb and Hund's rule exchange interactions in the UAL Model. The conduction band and the two 5f bands were treated in the tight-binding approximation and the hybridization was treated as being independent of $\underline{k}$. The HO gap was evaluated from a self-consistency equation by an iterative method. The first-order phase boundary was determined by a direct comparison of the free energies of the two phases.

Data availability

The authors declare that all data supporting the findings of this study are available from the authors.

ACKNOWLEDGEMENTS

The work performed at Temple was supported by the US Department of Energy, Office of Basic Energy Sciences, Materials Science through the award DE-FG02-01ER45872. This work was partially supported by the Brazilian agencies CNPq, CAPES and FAPERGS.

AUTHOR CONTRIBUTIONS

E.J.C., S.G.M. and P.S.R. performed calculations. All authors contributed to the discussion, the design of the research, the analysis of the results, and the writing of the manuscript.

ADDITIONAL INFORMATION

Competing interests: The authors declare that they have no competing financial interests.

Publisher's note: Springer Nature remains neutral with regard to jurisdictional claims in published maps and institutional affiliations.

REFERENCES

1. Palstra, T. T. M. et al. Superconducting and magnetic transitions in the feavy-fermion system URu_2Si_2. *Phys. Rev. Lett.* **55**, 2727–2730 (1985).
2. Maple, M. B. et al. Partially gapped Fermi surface in the heavy-electron superconductor Uru_2Si_2. *Phys. Rev. Lett.* **56**, 185–188 (1986).
3. Schoenes, J., Schönenberger, C., Franse, J. J. M. & Menovsky, A. A. Hall-effect and resistivity study of the heavy-fermion system Uru_2Si_2. *Phys. Rev. B* **35**, 5375–5378 (1987).
4. Broholm, C. et al. Magnetic excitations and ordering in the heavy-electron superconductor URu_2Si_2. *Phys. Rev. Lett.* **58**, 1467–1470 (1987).
5. Amitsuka, H. et al. Effect of Pressure on tiny antiferromagnetic moment in the heavy-electron compound URu_2Si_2. *Phys. Rev. Lett.* **83**, 5114–5117 (1999).
6. Hassinger, E. et al. Temperature-pressure phase diagram of URu_2Si_2 from resistivity measurements and ac calorimetry: hidden order and Fermi-surface nesting. *Phys. Rev. B* **77**, 115117 (2008).
7. Kernavanois, N. et al. Investigation of the crystal structure of URu_2Si_2 by high-resolution X-ray diffraction. *Physica B* **259-261**, 648–649 (1999).
8. Tonegawa, S. et al. Direct observation of lattice symmetry breaking at the hidden-order transition in URu_2Si_2. *Nat. Commun.* **5**, 4188 (2014).

9. Tabata, C. et al. X-ray backscattering study of crystal lattice distortion in hidden order of URu_2Si_2. *Philos. Mag.* **94**, 3691–3701 (2014).
10. Santini, P. & Amoretti, G. Crystal field model of the magnetic properties of URu_2Si_2. *Phys. Rev. Lett.* **73**, 1027–1030 (1994).
11. Ohkawa, F. J. & Shimizu, H. J. Quadrupole and dipole orders in URu_2Si_2. *J. Phys. Condens. Matter* **11**, L519–L524 (1999).
12. Kiss, A. & Fazekas, P. Group theory and octupolar order in URu_2Si_2. *Phys. Rev. B* **71**, 054415 (2005).
13. Hanzawa, K. Hidden octupole order in URu_2Si_2. *J. Phys. Condens. Matter* **19**, 072202 (2007).
14. Haule, K. & Kotliar, G. Arrested Kondo effect and hidden order in URu_2Si_2. *Nat. Phys.* **5**, 796–799 (2009).
15. Cricchio, F., Bultmark, F., Granaas, O. & Nordstrom, L. Itinerant magnetic multipole moments of rank five as the hidden order in URu_2Si_2. *Phys. Rev. Lett.* **103**, 107202 (2009).
16. Ikeda, H. et al. Emergent rank-5 nematic order in URu_2Si_2. *Nat. Phys.* **8**, 528–533 (2012).
17. Amitsuka, H. et al. Resonant X-ray scattering study of hidden order in URu_2Si_2 using a low-stress single crystal. *J. Phys. Conf. Ser.* **200**, 012007 (2010).
18. Walker, H. C. et al. Resonant x-ray scattering study of the URu_2Si_2 hidden-order phase. *Phys. Rev. B* **83**, 193102 (2011).
19. Ikeda, H. & Ohashi, Y. Theory of unconventional spin density wave: a possible mechanism of the micromagnetism in U-based heavy fermion compounds. *Phys. Rev. Lett.* **81**, 3723–3726 (1998).
20. Varma, C. M. & Zhu, L. Helicity order: hidden order parameter in URu_2Si_2. *Phys. Rev. Lett.* **96**, 036405 (2006).
21. Pepin, C., Norman, M. R., Burdin, S. & Ferraz, A. Modulated spin liquid: a new paradigm for Uru_2Si_2. *Phys. Rev. Lett.* **106**, 106601 (2011).
22. Dubi, Y. & Balatsky, A. V. Hybridization wave as the "hidden order" in Uru_2Si_2. *Phys. Rev. Lett.* **106**, 086401 (2011).
23. Fujimoto, S. Spin nematic state as a candidate of the hidden order phase of URu_2Si_2. *Phys. Rev. Lett.* **106**, 196407 (2011).
24. Flint, R., Chandra, P. & Coleman, P. Hastatic order in the heavy-fermion compound URu_2Si_2. *Nature* **493**, 621–626 (2013).
25. Kiselev, E. I., Scheurer, M. S., Wolfle, P. & Schmalian, J. Limits on dynamically generated spin-orbit coupling: absence of l = 1 Pomeranchuk instabilities in metals. *Phys. Rev. B* **95**, 125122 (2017).
26. Yoshida, R. et al. Signature of hidden order and evidence for periodicity modification in URu_2Si_2. *Phys. Rev. B* **82**, 205108 (2010).
27. Bareille, C. et al. Momentum-resolved hidden-order gap reveals symmetry breaking and origin of entropy loss in URu_2Si_2. *Nat. Commun.* **5**, 4326 (2014).
28. Hassinger, E. et al. Similarity of the Fermi surface in the hidden order state and in the antiferromagnetic state of URu_2Si_2. *Phys. Rev. Lett.* **105**, 216409 (2010).
29. Su, J.-J., Dubi, Y., Wolfle, P. & Balatsky, A. V. A charge density wave in the hidden order state of URu_2Si_2. *J. Phys. Condens. Matter* **23**, 094214 (2011).
30. Chandra, P., Coleman, P. & Flint, R. Hastatic order in URu_2Si_2: hybridization with a twist. *Phys. Rev. B* **91**, 205103 (2015).
31. Rau, J. G. & Kee, H.-Y. Hidden and antiferromagnetic order as a rank-5 superspin in URu_2Si_2. *Phys. Rev. B* **85**, 245112 (2012).
32. Das, P. et al. Absence of a static in-plane magnetic moment in the'hidden-order' phase of URu_2Si_2. *New. J. Phys.* **15**, 053031 (2013).
33. Metoki, N. et al. Neutron scattering experiments for the study of in-plane ordered moment in URu_2Si_2. *J. Phys. Soc. Jpn.* **82**, 055004 (2013).
34. Ross, K. A. et al. Strict limit on in-plane ordered magnetic dipole moment in URu_2Si_2. *Phys. Rev. B* **89**, 155122 (2014).
35. Mydosh, J. A. & Oppeneer, P. M. Colloquium: hidden order, superconductivity, and magnetism: the unsolved case of URu_2Si_2. *Rev. Mod. Phys.* **83**, 241102 (2011).
36. Mydosh, J. A. & Oppeneer, P. M. Hidden order behaviour in URu_2Si_2 (A critical review of the status of hidden order in 2014). *Philos. Mag.* **94**, 3642–3662 (2014).
37. Riseborough, P. S., Coqblin, B. & Magalhaes, S. G. Phase transition arising from the underscreened Anderson lattice model: a candidate concept for explaining hidden order in URu_2Si_2. *Phys. Rev. B* **85**, 165116 (2012).
38. Butch, N. P. et al. Symmetry and correlations underlying hidden order in URu_2Si_2. *Phys. Rev. B* **91**, 035128 (2015).
39. Wray, L. A. et al. Spectroscopic determination of the atomic f-electron symmetry underlying hidden order in URu_2Si_2. *Phys. Rev. Lett.* **114**, 236401 (2015).
40. Jeffries, J. R., Moore, K. T., Butch, N. P. & Maple, M. B. Degree of 5f electron localization in URu_2Si_2: electron energy-loss spectroscopy and spin-orbit sum rule analysis. *Phys. Rev. B* **82**, 033103 (2010).
41. Booth, C. H. et al. Multiconfigurational nature of 5f orbitals in uranium and plutonium intermetallics. *Proc. Natl. Acad. Sci. USA* **109**, 10205–10209 (2012).
42. Booth, C. H. et al. Probing 5f-state configurations in URu_2Si_2 with U L-III-edge resonant x-ray emission spectroscopy. *Phys. Rev. B* **94**, 045121 (2016).
43. Park, W. K. et al. Observation of the hybridization gap and Fano resonance in the Kondo lattice URu_2Si_2. *Phys. Rev. Lett.* **108**, 246403 (2012).
44. Denlinger, J. D. et al. Comparative study of the electronic structure of XRu_2Si_2: probing the Anderson lattice. *J. Electron Spectros. Relat. Phenomena* **117**, 347–369 (2001).
45. Oppeneer, P. M. et al. Electronic structure theory of the hidden-order material URu_2Si_2. *Phys. Rev. B* **82**, 205103 (2010).
46. Nozieres, P. Magnetic-impurities and Kondo effect. *Ann. Phys* **10**, 19–35 (1985).
47. Millis, A. J. & Lee, P. A. Large-orbital-degeneracy expansion for the lattice Anderson model. *Phys. Rev. B* **35**, 3394–3413 (1987).
48. Nozieres, P. & Blandin, A. M. Kondo effect in real metals. *J. Phys. (Paris)* **41**, 193–211 (1980).
49. Kung, H.-H. et al. Chirality density wave of the "hidden order" phase in URu_2Si_2. *Science* **347**, 1339–1342 (2015).
50. Schemm, E. R. et al. Evidence for broken time-reversal symmetry in the superconducting phase of URu_2Si_2. *Phys. Rev. B* **91**, 140506 (2015).
51. Matsuda, K., Kohori, Y., Kohara, T., Kuwahara, K. & Amitsuka, H. Spatially inhomogeneous development of antiferromagnetism in URu_2Si_2: evidence from Si-29 NMR under pressure. *Phys. Rev. Lett.* **87**, 087203 (2001).
52. Baek, S.-H. et al. Antiferromagnetic patches and hidden order in Uru_2Si_2 by impurity doping. *Phys. Rev. B* **81**, 132404 (2010).
53. Niklowitz, P. G. et al. Parasitic small-moment antiferromagnetism and nonlinear coupling of hidden order and antiferromagnetism in URu_2Si_2 observed by Larmor diffraction. *Phys. Rev. Lett.* **104**, 106406 (2010).
54. Pfleiderer, C., Mydosh, J. A. & Vojta, M. Pressure dependence of the magnetization of URu_2Si_2. *Phys. Rev. B* **74**, 104412 (2006).
55. Jaime, M., Kim, K. H., Jorge, G., McCall, S. & Mydosh, J. A. High magnetic field studies of the hidden order transition in URu_2Si_2. *Phys. Rev. Lett.* **89**, 287201 (2002).
56. Correa, V. F. et al. High-magnetic-field lattice length changes in URu_2Si_2. *Phys. Rev. Lett.* **109**, 246405 (2012).
57. Okazaki, R. et al. Rotational symmetry breaking in the hidden-order phase of URu_2Si_2. *Science* **331**, 439–442 (2011).
58. Ramirez, A. P. et al. Nonlinear susceptibility as a probe of tensor spin order in URu_2Si_2. *Phys. Rev. Lett.* **68**, 2680–2683 (1992).
59. Levallois, J., Behnia, K., Flouquet, J., Lejay, P. & Proust, C. On the destruction of the hidden order in URu_2Si_2 by a strong magnetic field. *Europhys. Lett.* **85**, 27003 (2009).
60. Altarawneh, M. M. et al. Sequential Spin polarization of the Fermi surface pockets in URu_2Si_2 and its implications for the hidden order. *Phys. Rev. Lett.* **106**, 146403 (2011).
61. Aynajian, P. et al. Visualizing the formation of the Kondo lattice and the hidden order in URu_2Si_2. *Proc. Nat. Acad. Sci.* **107**, 10383 (2010).
62. Werwinski, M., Rusz, J., Mydosh, J. A. & Oppeneer, P. M. Exceptional Ising magnetic behavior of itinerant spin-polarized carriers in URu_2Si_2. *Phys. Rev. B* **90**, 064430 (2014).